Journal Name

All-Solid-State Interpenetrating Network Polymer Electrolytes for Long Cycle Life of Lithium Metal Batteries¶

Received 00th January 20xx,
Accepted 00th January 20xx

DOI: 10.1039/x0xx00000x

www.rsc.org/

Yongfen Tong* [a,b], Hailong Lyu [b], Yuzhong Xu [a], Bishnu Prasad Thapaliya [b,c], Peipei Li [b], Xiao-Guang Sun* [b] and Sheng Dai* [b,c]

A star-shape polymer of 3-armed poly(ethylene glycol) methyl ether methacrylate-co-glycidyl methacrylate copolymer (3PPEGM-co-GMA) was synthesized using an atom transfer radical polymerization (ATRP) technique. All-solid-state interpenetrating network polymer electrolytes (INSPEs) were fabricated by simultaneous reaction of 3PPEGM-co-GMA and bisphenol A diglycidyl ether (BPDE) with polyetherdiamine (ED2003) in the presence of lithium bis(trifluoromethane) sulfonamide (LiTFSI). The INSPEs exhibited ionic conductivities higher than 10^{-5} S cm^{-1} at room temperature, a high oxidation stability of 4.5 *vs.* Li/Li^+ and remarkable stability towards lithium metal. Li metal batteries with $LiFePO_4$ as the cathode and INSPEs as the electrolyte cycled at a current rate of 0.1C at 60 °C showed a high initial discharge capacity of 156.2 mA h g^{-1} and a stable cycling performance over 200 cycles with a high coulombic efficiency of 99%. The results demonstrate that the interpenetrating network polymer electrolytes are promising electrolytes for next generation lithium-based batteries with high ionic conductivity, improved safety, and stable electrochemical performance.

1. Introduction

Although lithium ion batteries have been widely used in various portable electronic devices, electric vehicles and other electric energy storage systems, their energy densities still need to be significantly improved to meet those demands. [1, 2] Among various options, Li metal with a high theoretical specific capacity of 3860 mAh g^{-1} has attracted extensive attention as the anode in rechargeable lithium metal batteries.[3-6] Unfortunately, the undesired lithium dendrite growth in liquid electrolytes during cycling has prevented the practical use of Li metal anode in rechargeable batteries.[6-8] Currently, various approaches such as liquid electrolytes with functional additives, anode modification, [9, 10] minimizing volume change with stable hosts, [10, 11] or solid electrolytes [6, 9, 12-14] have been used to suppress lithium dendrite growth. Among different approaches, solid polymer electrolytes are the most promising candidates because of their high safety, flexibility in tuning the mechanical strength *via* structure design, easy adaption of volumetric change during cycling, and electrolyte leakage-proof.[15-19] So far, most studies have focused on polymers containing ethylene oxide moieties for an all-solid cell construction because of their ability to dissolve lithium salts and transport lithium ion. Unfortunately, polyethylene oxide (PEO) has high melting point of about 55 ˚C and its room temperature ionic conductivity is only ~10^{-7} S cm^{-1}, which is too low for practical applications.[20-22] To suppress the crystallinity of the PEO segments and improve the ambient temperature ionic conductivities, block copolymers, graft, comb-branched polymers with more flexible oligomeric EO side chains, and alternative polymer hosts have been synthesized.[23-38] However, the enhanced room temperature ionic conductivity was usually accompanied by decreased mechanical properties of the polymer electrolytes.

As crosslinking or formation of interpenetrating network is an effective way to enhance the mechanical strength of the polymer electrolytes,[39-46] herein we report a novel all-solid-state polymer electrolyte with an interpenetrating network prepared *via* a one-pot synthetic strategy using a ring-opening polymerization technique (**Scheme 1).** 3-arm poly (ethylene glycol) methyl ether methacrylate-co-glycidyl methacrylate copolymer (3PPEG-co-GMA) and bisphenol A diglycidyl ether (BPDE) were simultaneously cross-linked with polyetherdiamine (ED2003) to form an interpenetrating network. The interpenetrating network solid polymer electrolytes (INSPEs) not only exhibited high ionic conductivity, high flexibility and allowed homogeneous current distribution to effectively suppress Li dendrite growth, but also had good compatibility with cathodes and could be easily processed. The $LiFePO_4$ based Li metal batteries using the INSPEs exhibited superior electrochemical performance.

[a] *School of Environmental and Chemical Engineering, Nanchang Hangkong University, 696 Fenghe South Avenue, Nanchang 330063, China. E-mail address: yongfentong@nchu.edu.cn (Y. Tong)*
[b] *Chemical Science Division Oak Ridge National Laboratory, Oak Ridge, TN 37831, USA. E-mail address: sunx@ornl.gov (X. G. Sun); dais@ornl.gov (S. Dai).*
[c] *Department of Chemistry, University of Tennessee, Knoxville, TN 37996, USA*

2. Experimental

2.1 Materials

Trimethylolpropane (Acros Organics, 99%), α-Bromoisobutyryl bromide (98%), glycidyl methacrylate (GMA, ≥97.0%, GC), lithium bis(trifluoromethane)sulfonamide (LiTFSI, $CF_3SO_2NLi\text{-}SO_2CF_3$, battery grade), $LiPF_6$ (battery grade), copper (I) bromide (CuBr, 98%), poly (ethylene glycol) methyl ether methacrylate (PEGMA, M_n=500), 1, 1, 4, 7, 10, 10-hexamethyl triethylene tetramine (HMTETA), bisphenol A diglycidyl ether (BPDE) and Poly(propylene glycol)-*block*-poly(ethylene glycol)-*block*-poly(propylene glycol) bis(2-aminopropyl ether) (ED2003, average M_n ~2,000) were purchased from Sigma-Aldrich and used as received. All the solvents were anhydrous without further treatment.

2.2 Synthesis of copolymer 3PPEG-co-GMA-x by ATRP

The synthesis of 3-armed poly (ethylene glycol) methyl ether methacrylate-co-glycidyl methacrylate copolymer (3PPEG-co-GMA-x) is shown in **Scheme 1**. In a typical polymerization, a macro-initiator prepared according to previous procedure,[47] trimethylolpropane tri(2-bromo isobutyrate) ($TMPBr_3$, 0.14 g, 0.72 mmol equiv. Br), PEGMA (18.0 g, 36 mmol), GMA(1.02 g, 7.2 mmol), ligand HMTETA (165 mg, 0.72 mmol), CuBr (103 mg, 0.72 mmol), and anhydrous toluene (10 mL) were charged into a Schlenk flask under nitrogen. The solution was degassed three times with freeze-pump-thaw cycle. The flask was immersed in an oil bath preheated at 85 °C, and after 4 h it was quenched in liquid nitrogen. The solution was diluted with THF and passed through a column of neutral alumina to remove the copper salts. The product was precipitated twice from an excess of ether, filtered, and vacuum dried at 45 °C to obtain a colloidal product. ^{1}H NMR (δ_{ppm}, $CDCl_3$): 4.07 (s, 6H), 3.97 (d, 2H), 3.66(m, $-OCH_2CH_2O-$), 3.27 (d, 2H), 2.82(s, 1H, cyclic ether), 2.63 (s, 1H, cyclic ether), 1.59 (s, $-CH_3$), 0.94 (d, 2H), 0.86 (s, 3H). A series of star polymers, 3PPEG-co-GMA-x (x is the feed ratio of GMA by molar mass), were prepared by fixing the amount of PEGMA but varying the amount of GMA. The details of the feeding ratio are shown in **Table1**.

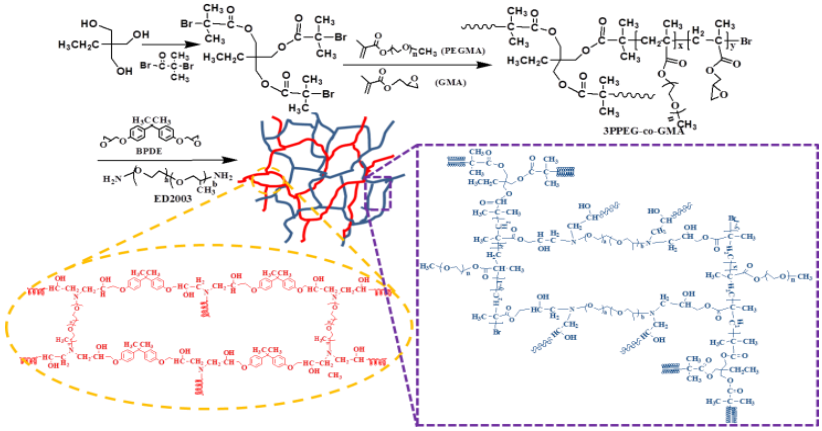

Scheme 1. Synthesis of the interpenetrating network solid polymer membrane (INSPM-x).

2.3 Synthesis of interpenetrating network all-solid-state polymer membranes (INSPMs)

A one-pot synthesis strategy based on a ring-opening polymerization reaction was used to prepare all-solid-state polymer membranes. 3PPEG-co-GMA-x, with varying amount of bisphenol A diglycidyl ether (BPDE), ED2003, and calculated amount of LiTFSI were successively added into the CH_3CN solution and the precursor solution was stirred at 25 °C for 12 h. Subsequently, the precursor solution was casted on a polytetrafluorethylene coated dish and heated at 80 °C for 24 h to ensure that all the epoxy groups were reacted. After that, it was further dried under high vacuum at 80 °C for 24 h. The thickness of obtained membrane is around 150 µm.

2.4 Characterization

Infrared (IR) spectroscopy was collected on a PerkinElmer FT-IR Spectrometer in the range of 4000-400 cm^{-1}. The ^{1}H NMR spectra were obtained on a Bruker spectrometer (400MHz) by using deuterated chloroform as the internal reference. The gel permeation chromatography (GPC), so-called size-exclusion chromatography (SEC) analysis, was conducted with a Breeze Waters system equipped with a Rheodyne injector, a 1515 Isocratic pump and a Waters 2414 differential refractometer using polystyrenes as the standard and tetrahydrofuran as the eluent at a flow rate of 1.0 mL/min and 40 °C through a Styragel column set, Styragel HT3 and HT4 (19 mm × 300 mm, 10^3 +10^4 Å) to separate molecular weight (MW) ranging from 10^2 to 10^6. X-ray diffraction (XRD) patterns were recorded on a Siemens D5005 diffraction meter with Ni-filtered Cu Kα radiation operating at 40 kV and 40 mA. The surface image of the membranes was investigated by scanning electron microscope (SEM), using an Environmental Scanning Electron Microscope (ESEM, FEI Quanta 200), the composite films were gold-sprayed prior to the measurements. Differential scanning calorimetric (DSC) measurements were performed using a TA DSC Q2000 differential scanning calorimeter. The samples were sealed in Al pans inside a glovebox. The samples were measured under a continuous nitrogen purge of 50 mL / min. The samples were cooled from room temperature to -90 °C, equilibrated, and then heated to 100 °C at a heating rate of 10 °C /min; then it was cooled to ‐ 90 °C again, equilibrated and finally heated to 100 °C at a heating rate of 10 °C / min. Thermogravimetric (TGA) measurements were performed on a TA 2950 thermogravimetric analyzer under a nitrogen flow of 50 mL min^{-1} from room temperature to 50 °C, isothermal for 30 min, and then heated from 50 to 600 °C at a heating rate of 10 °C min^{-1}.

The dynamic moduli and stress-strain properties of the polymer membranes were measured on a dynamic mechanical analyzer (DMA Q800). Polymer membrane was cut into rectangular size (4.0 mm x 3.0 mm) for dynamical mechanical analysis. Storage and loss modulus were measured with tension clamp utilizing a single frequency at a fixed strain of 0.01 N. Dynamic moduli tests were conducted from -100˚C to 100˚C at a heating rate of 3 K/min. Stress-strain analysis was conducted under controlled force mode at 25˚C with force ramp rate of 0.2 N/min.

Table1 Physical properties of 3PPEG-co-GMA-x and the corresponding interpenetrating network solid polymer membranes.

Sample	$TMPBr_3$: PEGMA: GMA[a]	$M_{n,GPC}$[b] (g/mol)	M_w/M_n[b]	T_g,°C	T_m (˚C)	ΔH_m (J/g)
3PPEG-co-GMA-30	1:100:30	27542	1.06	-63.1	-	-
3PPEG-co-GMA-60	1:100:60	30199	1.04	-62.8	-	-
3PPEG-co-GMA-90	1:100:90	32287	1.10	-61.2	-	-
INSPM-30	-	-	-	-55.2	34.7	-87.4
INSPM-60	-	-	-	-56.2	33.7	-64.6
INSPM-90	-	-	-	-57.8	33.7	-59.3

[a] Feed ratio of trimethylolpropane-tri(2-bromoisobutyrate) ($TMPBr_3$) to poly(ethylene glycol) methyl ether methacrylate (PEGMA) and glycidyl methacrylate (GMA) by molar mass. [b] Determined by GPC calibrated with polystyrene standards.

2.5 Electrochemical measurements

Alternating current (AC) impedance measurement was carried out using a Swagelok cell on a Bio-Logic VSP instrument over a frequency range of 1 MHz to 100 mHz with a perturbation amplitude of 10 mv. The samples are equilibrated at each temperature for at least 90 min before measurement. The ionic conductivity (σ) of the polymer electrolytes was calculated according to the following equation:

$$\sigma = \frac{L}{R \cdot S} \quad (1)$$

where R is the bulk electrolyte resistance, L and S are the thickness and area of the polymer electrolyte film, respectively. The real part of dielectric constant was calculated by using following equation:

$$\varepsilon' = \frac{C_p L}{\varepsilon_0 S} \quad (2)$$

where *C*p is the capacitance of the sample, ε_0 (dielectric permittivity in vacuum) is equal to 8.85 x 10^{-12} F/m, *S* is the effective surface area, and *L* is the thickness of the samples.

Linear sweep voltammetry (LSV) was carried out using a Pt || Polymer electrolyte || Li Swagelok cell from 2.0 to 6 V *vs.* Li/Li^+ at 60 °C with a scan rate of 10 mV s^{-1}. The lithium transference number (t_+) was determined by using a combination method of dc polarization and ac impedance measurements. [48] The sample was sandwiched between two 0.5 mm-thick lithium foils as non-blocking electrodes in an argon gas-filled glove box. The dc voltage pulse applied to the cell was 10 mV. It can be obtained according to the following equation:

$$t_+ = \frac{I_s(\Delta V - I_0 R_0)}{I_0(\Delta V - I_s R_s)} \quad (3)$$

Where Δ*V* is the potential applied across the cell, I_0 and I_s are the initial current and steady-state current, R_0 and R_s are the charge transfer resistance before and after the polarization.

To test the stability of the polymer electrolytes against lithium metal, symmetric Li||Li cells were assembled and cycled under a sequence of 3 hrs charge under a current density of 0.2 mA cm^{-2}, 1 hr rest, 3 hrs discharge under a current density of -0.2 mA cm^{-2} and 1hr rest. $LiFePO_4$ electrodes were prepared by first homogeneously mixing $LiFePO_4$ powder and C45 in a LiTFSI/PEO (m_w, 1,000,000) (Li/EO = 1/10) solution in acetonitrile with the active material weight ratio of 5:1:4, and then coated onto an aluminum foil and dried at 100 °C for 12 h. The Loading of active material was about 1.0 mg cm^{-2}. Coin cells with lithium foil as anode and $LiFePO_4$ as cathode were assembled inside an argon-filled glove box with a moisture level < 1 ppm. Cycling performance of the polymer electrolytes was evaluated on an Arbin BT2000 instrument over the voltage range of 2.5 - 4.0 V at 60 °C.

3. Results and discussion

3.1 Structural Characterization

As shown in **Scheme 1,** both 3PPEG-co-GMA-x and BPDE can react with ED2003 intramolecularly to form large and small closed loop, respectively, during which process the two loops can interpenetrate each other. In addition, both 3PPEG-co-GMA-x and BPDE can react with ED2003 intermolecularly to form crossed networks. Overall, the two processes resulted in interpenetrating network solid polymer membranes (INSPM), which are referred as INSPM-x.

The ring-opening polymerization of the 3PPEG-co-GMA-60 and ED2003 was confirmed by the FT-IR spectra. As a baseline, a polymer (ED2003-BPDE) based on the same reaction of epoxy and diamine was synthesized using BPDE and ED2003. As shown in the **Fig.1**, the broad peak due to the N-H stretching vibration was observed around 3500 and 2870 cm^{-1} in both ED2003-BPDE and INSPM-60 network system. The peaks at 1610 and 1514 cm^{-1} were ascribed to the C-C stretching of the benzene rings from the aromatic components and the peaks at 1245 and 836 cm^{-1} could be

assigned to the aromatic ethers of BPDE. The peak at 1090 was related to the C-O-C stretching vibration in 3PPEG-co-GMA-60 and ED2003. The peaks corresponding to epoxy stretching at 930 and 783cm^{-1} were observed in 3PPEG-co-GMA-60, whereas they were not observed in both ED2003-BPDE and INSPM-60. Instead the new peaks at 1653 and 946 cm^{-1} in the latter two samples confirmed the formation of C-N bond. All the above signature peaks confirmed that the cross-linking reactions between the amine groups in ED2003 and the epoxy groups in both BPDE and 3PPEG-co-GMA-60 indeed proceed to form interpenetrating network polymer structures.

The thermal stability of the sample was evaluated by thermogravimetric analysis (TGA). **Fig. 2a** shows a single step decomposition around 350 °C for INSPM-x-LiTFSI. The typically reported thermal stability of ethylene oxide (EO) or propylene oxide (PO) unit based polymers in nitrogen atmosphere was around 200 °C with rapid decomposition around 220-300 °C.[49, 50] The increased thermal stability of the interpenetrating network polymer electrolyte, higher than that of PEO or PPO based electrolyte, could be attributed to the formation of network structure and the ester bonds in the polymer backbone. It indicates that the polymer electrolytes are highly stable and safe to be used at higher temperatures.

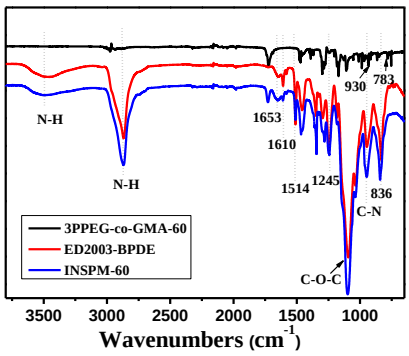

Fig. 1. FT-IR spectra of 3PPEG-co-GMA-60, ED2003-BPDE and INSPM-60.

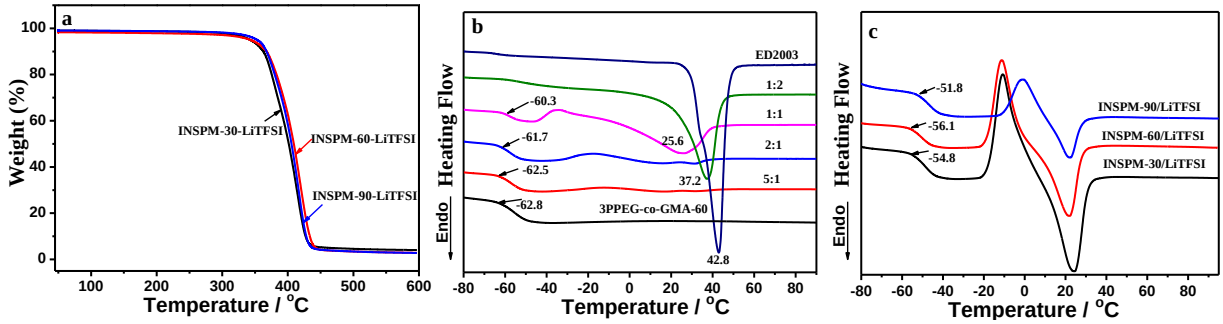

Fig. 2. (a) TGA thermogram of NISPM-x-LiTFSI under nitrogen at a heating rate of 10 °C min^{-1}, (b) DSC curves of cross-linking solid state polymers based on 3PPEG-co-GMA-x and ED2003 under nitrogen during the second heating scan at a scan rate of 10 °C min^{-1}, the molar ratio of the epoxy and amino is 5:1, 2:1, 1:1 and 1:2, respectively and (c) DSC curves of INSPM-x/LiTFSI electrolytes.

The melting temperature (T_m) and glass transition temperature (T_g) are important parameters to measure the degree of crystallinity and flexibility of the polymer electrolytes. All the differential scanning calorimetry (DSC) curves of the copolymers and polymer electrolyte membranes were studied over the temperature range from - 90 to 100 °C. As can be seen from **Table1**, 3PPEG-co-GMA-x had a T_g around -62 °C without apparent melting peaks, proving that the star copolymers are amorphous. To investigate the effect of cross-linking density on the thermal properties of the interpenetrating network membranes, samples base on epoxy 3PPEG-co-GMA-60 and different amount of diamine ED2003 were prepared. As shown in **Fig. 2b,** when the molar ratio of the epoxy and amino was higher than 2:1, the cross-linked polymer maintained an amorphous state. Increasing the amount of ED2003 resulted in the increase of crystallinity. The melting point decreased from 42.8 °C for pure ED2003 to 37.2 °C for the sample with a molar ratio of the epoxy and amino of 1:2. Further increase the amount of 3PPEG-co-GMA-60 decreased the melting point further. In addition, the Tg gradually decreased with increasing the amount of ED2003, indicating that the cross-linking density influenced the mobility of the EO chains. The thermal properties of 3PPEG-co-GMA-30 and 3PPEG-co-GMA-90 crosslinked with ED2003 at a molar ratio of epoxy and amine of 2:1 were also studied, as shown in **Fig.S1**. All the membranes showed an obvious Tg

from – 63.3 °C to – 50.6 °C, indicating good chain mobility without significant crystallinity. Therefore, to maintain amorphous state with good chain mobility for higher ionic conductivity, a fixed molar ratio of 2:1 between epoxy and amino was used in the following experiments. Moreover, to further increase the mechanical strength, BPDE was also added in the interpenetrating network system with the same content of epoxy and amino in all cases. The DSC thermograms of the obtained membranes (INSPM-x) are shown in **Fig. S2** with the thermal parameters summarized in **Table 1,** in which ΔH_m was calculated from the integral area of the melting peak. As shown in **Fig.S2**, all the membranes showed a crystalline melting peak around 34 °C, apparently due to the melting temperature of the EO/PO segment in ED2003. It is worth mentioning that the enthalpy of $T_{m,EO}$ decreased with increasing of GA content in the star copolymer, that is, INSPM-90 showed the lowest crystallinity. It is because that less BPDE was added in the system with higher GA content in 3PPEG-co-GMA-90, indicating higher crosslinking between the star copolymer and ED2003. The thermal properties of INSPM-x doped with lithium salt were also investigated by DSC, and the typical DSC traces are shown in **Fig. 2c**. The decrease of melting temperature (T_m) to near room temperature coupled with the decreased heat of fusion (ΔH_m) of the interpenetrating network electrolytes indicated that the crystalline structures of the EO/PO segments were disrupted efficiently. At the same time, low glass transition temperatures (T_g) between -56.1 °C and - 51.8 °C were observed in all samples, suggesting high ion transport in the INSPM-x-LiTFSI systems at room temperature. Among all the samples investigated in this study, INSPM-60-LiTFSI exhibited the lowest T_g value of -56.1 °C. It indicated that proper crosslinking degree could inhibit the crystallization efficiently, whereas excessive cross-linking might be detrimental to the movement of the PEG chains and the ion mobilities.

X-ray diffraction (XRD) patterns of INSPM-x were obtained in order to check the crystallinity within the membranes (**Fig.S3**). The two intense peaks at 19° and 23° correspond to the crystallinity of the EO segments. With increasing the GA content in 3PPEG-co-GMA-x, these crystalline peaks decreased and eventually almost disappeared, indicating more amorphous phase in the polymer, in good agreement with the DSC results.

Figs. S4a & **b** show the typical images of INSPM-60-LiTFSI obtained by reaction between star polymer of 3PPEG-co-GMA-x, BPDE and ED2003 in the presence of LiTFSI. The membrane is self-standing and very flexible. **Fig. S4c** & **d** show the SEM images of the surface morphologies of the INSPM-60-LiTFSI electrolyte. As can be seen from the figures, the film showed a uniform surface without phase separation. As battery safety is always a concern for practical application, flammability of INSPM-60-LiTFSI and commercial liquid carbonate electrolyte (1 M $LiPF_6$ in EC/DMC/DEC = 1/1/1 v/v) were also evaluated. As shown in **Fig. S4e** & **f,** when ignited with fire, the liquid carbonate electrolyte exhibited a combustion behavior, whereas the INSPM-60-LiTFSI could be hardly ignited by the flame. The non-flammability of INSPM-60-LiTFSI suggests that it is a promising alternative to conventional liquid carbonate electrolytes for application in lithium metal battery.

Fig. S5a shows the stress as a function of strain for INSPM-60 at 25 °C with a force ramp rate of 0.2 N/min. It exhibited an almost perfect neo-Hookean behaviour and was broken at a stress of 1.23 MPa and a strain of 224% without yielding because of its chemical crosslinking nature. [51, 52] The storage and loss modulus measurement of INSPM-60 exhibited a modulus of 20 MPa at 20 °C **(Fig. 5b)**.

3.2 Ionic Conductivity

Fig. 3a shows the temperature dependence of the ionic conductivities of the INSPM-60-LiTFSI electrolytes with different salt concentrations. Generally, the temperature dependence of the ionic conductivity can be described by the Vogel-Tamman-Fulcher (VTF) equation:

$$\sigma T^{1/2} = A\exp\left(\frac{-E_a}{R(T-T_0)}\right) \quad (4)$$

where A is a frequency factor, E_a is an activation energy considered to be the barrier for ionic conduction, R is the ideal gas constant, and T_0 is the ideal transition temperature related to the glass transition temperature. As expected from the VTF equation, the ionic conductivities of all the electrolytes increased with increasing temperature (**Fig. S6**). It is found that the cross-linked polymer electrolytes with an [O]/[Li^+] ratio of 16 exhibited the maximum ionic conductivity. The initial increase of ionic conductivity with increase of [O]/[Li^+] ratio was mainly due to the increase of charge carrier. However,

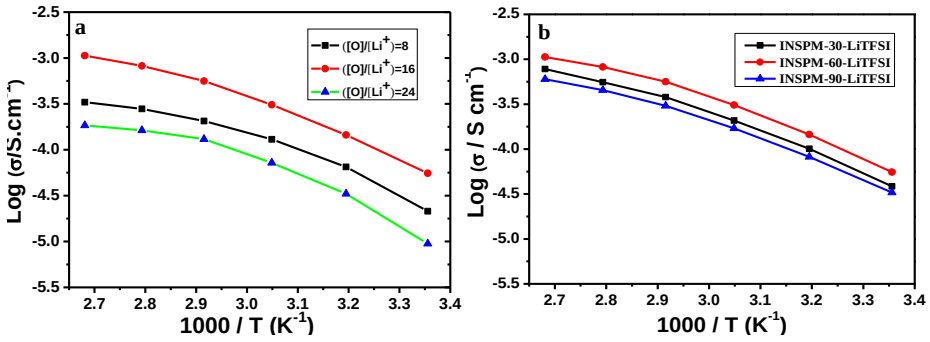

Fig. 3 Temperature dependence of ionic conductivity of (a) INSPM-60-LiTFSI with various [O]/ [Li^+] ratios and (b) INSPM-x/LiTFSI with [O]/ [Li^+] = 16.

further increase of salt concentration would lead to decreased ion mobility because of the concurrence of ion aggregates formation and glass transition temperature increase. The conductivity data were fitted according to the VTF equation and the corresponding parameters are listed in **Table S1.** The E_a values of INSPM-60-LiTFSI are around 9.0 kJ / mol, indicating facile ion transport in these amorphous polymer electrolytes.

Fig. 3b shows the temperature dependence of ionic conductivities for the INSPM-x-LiTFSI system at a constant salt concentration of [O]/[Li^+] = 16. INSPM-60-LiTFSI exhibited the maximum ionic conductivity of 5.6×10^{-5} S cm^{-1} and 1.1×10^{-3} S cm^{-1} at 25 and 100 °C, respectively. As mentioned earlier, the high ionic conductivity at room temperature was mainly due to the amorphous structure of the PEG segments in the star structure, consistent with the DSC results. In the INSPM-x-LiTFSI electrolytes, there are two kinds of ethylene oxide (EO) moieties: one is the EO unit in ED2003, whose mobility is restricted due to its participation in crosslinking reaction; the other one is the EO unit in 3PPEG-co-GMA-x, which has sufficient segmental motion due to the comb-like structure. The INSPM-60-LiTFSI not only had the optimum crosslinking density to provide the mechanical strength but also had sufficient segmental mobility to provide the maximum ionic conductivity.

Fig. S7 shows the frequency dependence of dielectric permittivity ε'(ω) for the interpenetrating network polymer electrolytes. The dipoles are not able to follow the external electric field at high frequencies, so the ε' value decreases gradually with increasing frequency, indicating underlying relaxations.[53, 54] While it is desirable for ion-conducting polymer systems to have high dielectric constants, the composition changes in the three samples seemed to have little influence on their ε' values, that is, 7.3, 7.3 and 5.6 for INSPM-30-LiTFSI, INSPM-60-LiTFSI and 5.5 for INSPM-90-LiTFSI, respectively, which are typical values for ethers and EO dominant polymer systems.[55, 56]

Lithium transference number (t_{Li^+}) was measured for the INSPM-60-LiTFSI membranes using AC impedance and Chronoamperometry.[48, 57-59] The typical polarization curve of the INSPM-60-LiTFSI electrolyte was shown in **Fig.S8a,** whereas the impedance spectroscopy under initial and steady-state current conditions were shown in the inset of **Fig.S8a**. According to Eq. (3), the calculated t_{Li^+} is 0.37, which is colse to the reported value in the literature.[17, 60-62]

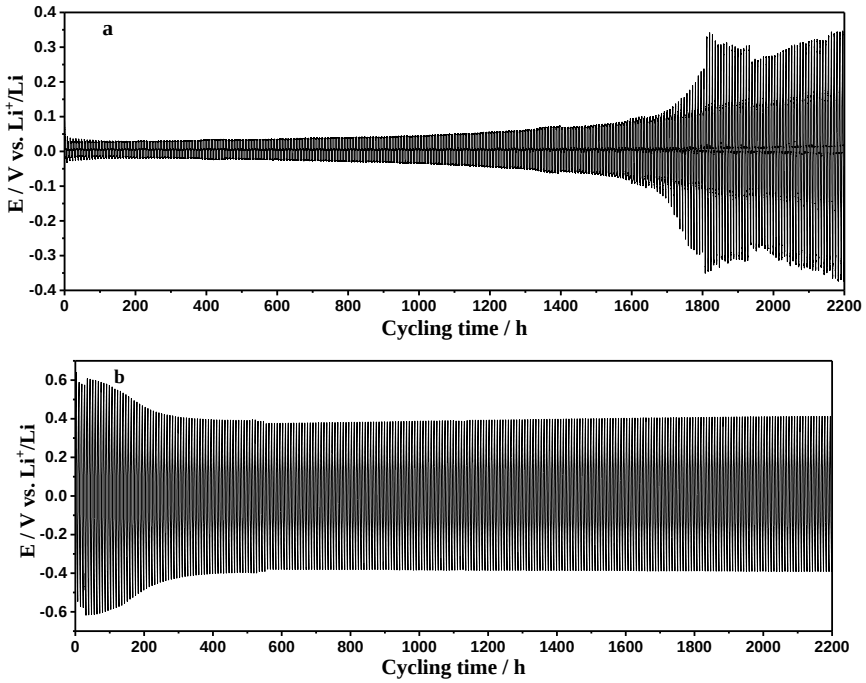

Fig. 4 Cycling performance of symmetric Li||Li cells in (a) 1.0 M $LiPF_6$/EC-DMC-DEC (1-1-1 in vol) and (b) INSPM-60-LiTFSI ([O]/ [Li] = 16) under a sequence of 3hrs charge at 0.2 mA cm-2, 1hr rest, 3 hrs discharge at 0.2 mA cm-2 and 1 hr rest at 60 °C.

3.3 Electrochemical and Interfacial Stability

Fig. S8b shows the linear sweep voltammograms of INSPM-x-LiTFSI electrolytes, which exhibited a very low current below 4.5 V *vs.* Li/Li^+. However, when the voltage was further increased, the current increased significantly, suggesting that the electrolytes have an electrochemical stability window of 4.5 V. This value is consistent with those reported for other polymer electrolytes used in rechargeable lithium polymer batteries.[40] As is well-known that for application in lithium metal batteries the polymer electrolytes must be stable against lithium metal electrode under charge-discharge conditions. Therefore, symmetric Li||Li cells were assembled with the INSPM-60-LiTFSI and liquid electrolyte, respectively and were cycled using a sequence of 3 hrs charge

under a current density of 0.2 mA cm^{-2}, 1 hr rest, 3 hrs discharge under a current density of 0.2 mA cm^{-2}, and 1 hr rest. **Fig. 4** shows the cycling performance of the two cells. The initial voltage is only 0.025 V for the cell in liquid electrolyte because of its high ionic conductivity. However, it gradually increased with cycling, reached 0.3 V after 1800 hrs and further increased with cycling, mainly due to the increased cell impedance resulting from the thickening of SEI layers during the repeated lithium deposition/stripping process (**Fig. 4a**). As a comparison, the cell in INSPM-60-LiTFSI exhibited an excellent cycling stability (**Fig. 4b)**. It exhibited an initial high voltage of 0.6 V due to the low ionic conductivity of the polymer electrolyte as compared to the liquid electrolyte, and also attributed to the reactions at the surfaces of the lithium electrodes and formation of the SEI layers. The cell voltage gradually decreased to 0.4 V after 300 hrs and was maintained even after 2200 hrs, demonstrating highly stable lithium plating/stripping behaviour. After cycling, the cell was disassembled inside the glovebox, and the surface morphology of the lithium metal and the polymer membrane were evaluated by SEM (**Fig. S9)**. The surface of the cycled polymer membrane was still smooth and exhibited no apparent defects, like that of fresh polymer membrane (**Fig. S9a** & **b)**. Compared with the fresh lithium anode (**Fig. S9c**), the cycled lithium electrode also exhibited compact and smooth morphology (**Fig. S9d**), which contributed to an improved cycling performance and a notable improvement in safety.

Comparing the cycling performance of the symmetric Li||Li cells in both liquid electrolyte and INSPM-60-LiTFSI, it seems that the modulus of the polymer membrane might not be the sole parameter to suppress lithium dendrite growth.[63] Although the polymer electrolytes, INSPM-60-LiTFSI had a modulus far less than that predicted in the model, it nonetheless allowed homogeneous current distribution and good adhesion to the lithium electrodes, which were important to suppress lithium dendrite growth but the latter was neglected in the original model. Also, it didn't account for the effect of the SEIs formed on the surface of the lithium electrodes, which would influence the current distribution during cycling as well as the initiation of lithium dendrite.[63]

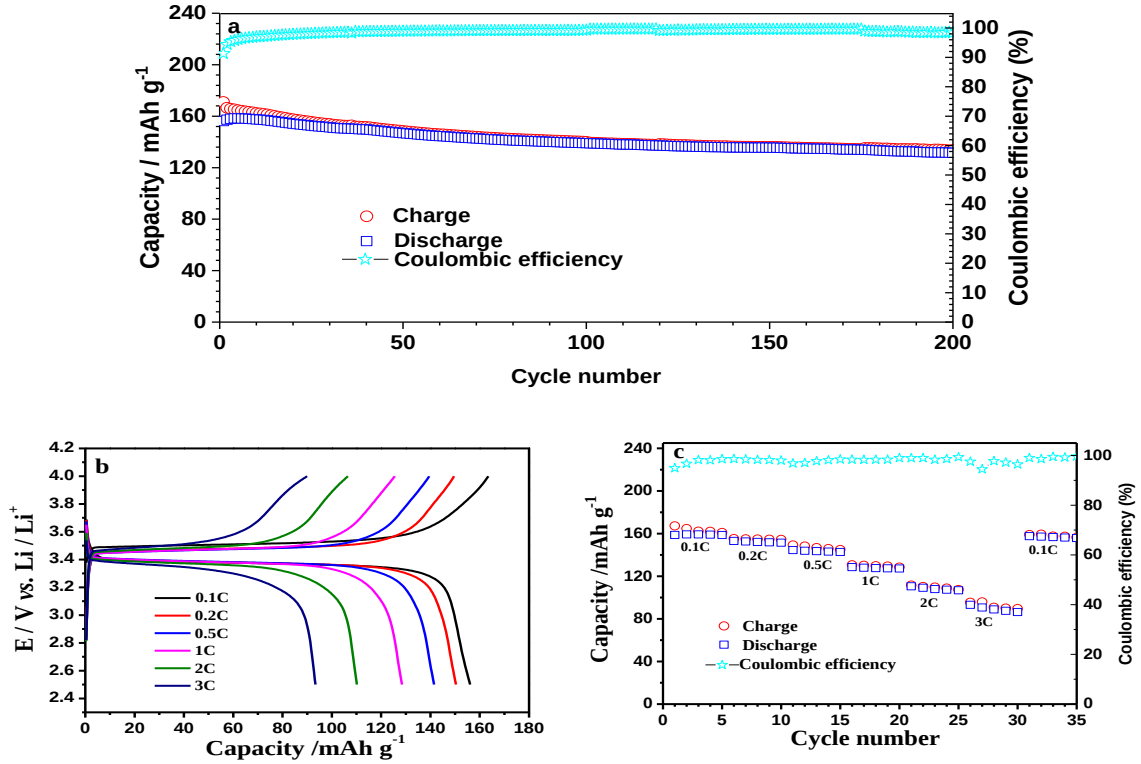

Fig. 5 Electrochemical performances of the batteries based on INSPM-60-LiTFSI electrolytes at 60 °C. (a) cycle performance of Li || INSPM-60-LiTFSI || $LiFePO_4$ cell at a current rate of 0.1C; (b) charge-discharge profiles and (c) the reversible capacity at various current rates (C/10 to 3C).

3.4 Charge-discharge behavior of the INSPM-x-LiTFSI electrolytes

The electrochemical performance of the lithium-ion cell with INSPM-60-LiTFSI electrolytes was evaluated by assembling coin cells using lithium metal as the anode and $LiFePO_4$ as the cathode. **Fig.5a** shows the long cycling performance of the cell under a current density of 0.1C at 60 °C. This performance is comparable to those previously reported systems, even some with liquid electrolytes (**Table S2**). The initial discharge capacity was 156.2 mAh g^{-1}, and it gradually increased and then decreased with cycling due to the activation of the cathode electrode and the formation of solid electrolyte interfaces. After 200 cycles, the reversible capacity was still as high as 132 mAh g^{-1}, about 84 % of its initial capacity. The coulombic efficiency was quickly increased to 96% within the five cycles and then gradually increased to and

maintained at 99% through the whole cycling process, indicating a remarkable stable cycle performance. **Fig.5b** illustrates the charge-discharge curves of the cell at different current rates, stepwise increase from 0.1 to 3.0 C and then return to 0.1 C. Generally, the discrepancy between the charge and discharge profile was small, that is, only 170 mV at a high current of 3C, indicating good lithium kinetics within the cathode that was facilitated by the high ionic conductivity of the polymer electrolyte. This is further demonstrated in **Fig.5c,** which shows the cycling performance of the cell based on INSPM-60-LiTFSI electrolyte at various C-rates. The reversible capacity was 158.7, 153.1, 144.6, 128.5, 110.5 and 93.5 mAh g^{-1} under the current density of C/10, C/5, C/2, 1.0 C, 2.0 C and 3.0C, respectively. When the current was returned to 0.1C, the reversible capacity was back to 157.6 mAh g^{-1}, indicating good reversibility of the battery.

4. Conclusion

In summary, novel network polymer electrolyte membranes were obtained *via* a ring-opening polymerization technique. The polymer electrolyte membranes were self-standing, flexible and non-tacky and could be successfully used as separators in Li metal batteries. The ionic conductivity of the polymer electrolytes could be easily optimized by varying the GMA content in the 3-arm prepolymer, the crosslinking density or lithium salt concentration. The electrolyte possessed a high electrochemical stability window of 4.5 V, had good stability to suppress Li dendrite growth in lithium metal batteries. Lithium metal batteries assembled using the polymer electrolyte as separator, $LiFePO_4$ as cathode exhibited a high capacity of 156.2 mAh g^{-1} under a current rate of 0.1C at 60 °C and long cycling stability. It also exhibited excellent rate capability up to 3C. Therefore, the excellent electrochemical properties of the interpenetrating network polymer electrolyte make it alternative promising electrolytes for the solid-state lithium-based batteries.

Conflicts of interest

There are no conflicts to declare.

Acknowledgements

This work was supported by the U.S. Department of Energy, Office of Science, Office of Basic Energy Sciences, Materials Sciences and Engineering Division under contract number DE-AC05-00OR22725. Y. Tong also acknowledges support from the China Scholarship Council (CSC) and Jiangxi Association for Science and Technology program.

References

1. E. Quartarone and P. Mustarelli, *Chem Soc Rev*, 2011, **40**, 2525-2540.
2. J.-M. Tarascon and M. Armand, *Nature*, 2001, **414**, 359-367.
3. P. G. Bruce, S. A. Freunberger, L. J. Hardwick and J. M. Tarascon, *Nat. Mater.*, 2012, **11**, 19-29.
4. Y. X. Yin, S. Xin, Y. G. Guo and L. J. Wan, *Angew. Chem. Inter. Ed.*, 2013, **52**, 13186-13200.
5. H. Kim, G. Jeong, Y. U. Kim, J. H. Kim, C. M. Park and H. J. Sohn, *Chem. Soc. Rev.*, 2013, **42**, 9011-9034.
6. W. Xu, J. L. Wang, F. Ding, X. L. Chen, E. Nasybutin, Y. H. Zhang and J. G. Zhang, *Energy Environ. Sci.*, 2014, **7**, 513-537.
7. Y. Y. Lu, Z. Y. Tu and L. A. Archer, *Nat. Mater.*, 2014, **13**, 961-969.
8. Y. Wang, W. H. Zhong, T. Schiff, A. Eyler and B. Li, *Adv. Energy Mater.*, 2015, **5**.
9. K. Zhang, G. H. Lee, M. Park, W. J. Li and Y. M. Kang, *Adv. Energy Mater.*, 2016, **6**.
10. D. C. Lin, Y. Y. Liu and Y. Cui, *Nat. Nanotech.*, 2017, **12**, 194-206.
11. X. X. Zeng, Y. X. Yin, N. W. Li, W. C. Du, Y. G. Guo and L. J. Wan, *J. Am. Chem. Soc.*, 2016, **138**, 15825-15828.
12. Y. F. Zhang, W. W. Cai, R. Rohan, M. Z. Pan, Y. Liu, X. P. Liu, C. C. Li, Y. B. Sun and H. S. Cheng, *J. Power Sources*, 2016, **306**, 152-161.
13. S. W. Liang, U. H. Choi, W. J. Liu, J. Runt and R. H. Colby, *Chem. Mater.*, 2012, **24**, 2316-2323.
14. Q. W. Pan, D. Barbash, D. M. Smith, H. Qi, S. E. Gleeson and C. Y. Li, *Adv. Energy Mater.*, 2017, **7**.
15. V. Di Noto, S. Lavina, G. A. Giffin, E. Negro and B. Scrosati, *Electrochim. Acta*, 2011, **57**, 4-13.
16. N. Kamaya, K. Homma, Y. Yamakawa, M. Hirayama, R. Kanno, M. Yonemura, T. Kamiyama, Y. Kato, S. Hama, K. Kawamoto and A. Mitsui, *Nat. Mater.*, 2011, **10**, 682-686.
17. R. Bouchet, S. Maria, R. Meziane, A. Aboulaich, L. Lienafa, J. P. Bonnet, T. N. T. Phan, D. Bertin, D. Gigmes, D. Devaux, R. Denoyel and M. Armand, *Nat. Mater.*, 2013, **12**, 452-457.
18. D. T. Hallinan and N. P. Balsara, in *Annual Review of Materials Research, Vol 43*, ed. D. R. Clarke, 2013, vol. 43, pp. 503-+.
19. H. Zhang, C. M. Li, M. Piszcz, E. Coya, T. Rojo, L. M. Rodriguez-Martinez, M. Armand and Z. B. Zhou, *Chem. Soc. Rev.*, 2017, **46**, 797-815.
20. C. Berthier, W. Gorecki, M. Minier, M. B. Armand, J. M. Chabagno and P. Rigaud, *Solid State Ionics*, 1983, **11**, 91-95.
21. B. K. Choi and Y. W. Kim, *Electrochim. Acta*, 2004, **49**, 2307-2313.
22. M. Marzantowicz, J. R. Dygas, F. Krok, Z. Florjanczyk and E. Zygadlo-Monikowska, *J. Non-Crystal. Solids*, 2006, **352**, 5216-5223.
23. A. Panday, S. Mullin, E. D. Gomez, N. Wanakule, V. L. Chen, A. Hexemer, J. Pople and N. P. Balsara, *Macromolecules*, 2009, **42**, 4632-4637.
24. M. Singh, O. Odusanya, G. M. Wilmes, H. B. Eitouni, E. D. Gomez, A. J. Patel, V. L. Chen, M. J. Park, P. Fragouli, H. Iatrou, N. Hadjichristidis, D. Cookson and N. P. Balsara, *Macromolecules*, 2007, **40**, 4578-4585.
25. W. S. Young, W. F. Kuan and T. H. Epps, *J. Polym. Sci. B-Polym. Phys.*, 2014, **52**, 1-16.
26. X. Li, J. Iocozzia, Y. H. Chen, S. Q. Zhao, X. Cui, W. Wang, H. F. Yu, S. L. Lin and Z. Q. Lin, *Angew. Chem. Int. Ed.*, 2018, **57**, 2046-2070.
27. X. G. Sun, J. Hou and J. B. Kerr, *Electrochim. Acta*, 2005, **50**, 1139-1147.
28. N. Yoshimoto, O. Shimamura, T. Nishimura, M. Egashira, M. Nishioka and M. Morita, *Electrochem. Commun.*, 2009, **11**, 481-483.
29. X. Zuo, X. M. Liu, F. Cai, H. Yang, X. D. Shen and G. Liu, *J. Mater. Chem.*, 2012, **22**, 22265-22271.
30. X. G. Sun and J. B. Kerr, *Macromolecules*, 2006, **39**, 362-372.
31. G. Allegra and F. Ganazzoli, *Prog. Polym. Sci.*, 1991, **16**, 463-508.
32. K. Inoue, *Prog. Polym. Sci.*, 2000, **25**, 453-571.
33. X. G. Sun, J. B. Kerr, C. L. Reeder, G. Liu and Y. B. Han, *Macromolecules*, 2004, **37**, 5133-5135.
34. T. Niitani, M. Amaike, H. Nakano, K. Dokko and K. Kanamura, *J. Electrochem. Soc.*, 2009, **156**, A577-A583.
35. X. G. Sun, C. L. Reeder and J. B. Kerr, *Macromolecules*, 2004,

37, 2219-2227.
36. Q. Ma, H. Zhang, C. W. Zhou, L. P. Zheng, P. F. Cheng, J. Nie, W. F. Feng, Y. S. Hu, H. Li, X. J. Huang, L. Q. Chen, M. Armand and Z. B. Zhou, *Angew. Chem. Int. Ed.*, 2016, **55**, 2521-2525.
37. K. Kimura, M. Yajima and Y. Tominaga, *Electrochem. Commun.*, 2016, **66**, 46-48.
38. Y. Tominaga and K. Yamazaki, *Chem. Commun.*, 2014, **50**, 4448-4450.
39. X. C. Liu, G. L. Ding, X. H. Zhou, S. Z. Li, W. S. He, J. C. Chai, C. G. Pang, Z. H. Liu and G. L. Cui, *J. Mater. Chem. A*, 2017, **5**, 11124-11130.
40. J. R. Nair, M. Destro, F. Bella, G. B. Appetecchi and C. Gerbaldi, *J. Power Sources*, 2016, **306**, 258-267.
41. P. Basak and S. V. Manorama, *J. Macromol. Sci. -Pure and Appl. Chem.* , 2006, **A43**, 369-382.
42. A. M. Elmer and P. Jannasch, *Solid State Ionics*, 2006, **177**, 573-579.
43. D. Luo, Y. Li, W. L. Li and M. J. Yang, *J. Appl. Polymer Scie.*, 2008, **108**, 2095-2100.
44. H. J. Ha, E. H. Kil, Y. H. Kwon, J. Y. Kim, C. K. Lee and S. Y. Lee, *Energy Environmental Sci.*, 2012, **5**, 6491-6499.
45. P. L. Kuo, C. A. Wu, C. Y. Lu, C. H. Tsao, C. H. Hsu and S. S. Hou, *Acs Appl. Mater. Interfaces*, 2014, **6**, 3156-3162.
46. Q. J. Wang, W. L. Song, L. Z. Fan and Q. Shi, *J. Power Sources*, 2015, **295**, 139-148.
47. Y. F. Tong, L. Chen, X. H. He and Y. W. Chen, *J. Power Sources*, 2014, **247**, 786-793.
48. P. G. Bruce and C. A. Vincent, *J. Electroanal. Chem.*, 1987, **225**, 1-17.
49. T. Shodai, B. B. Owens, H. Ohtsuka and J. Yamaki, *J. Electrochem. Soc.*, 1994, **141**, 2978-2981.
50. S. Han, C. Kim and D. Kwon, *Polymer*, 1997, **38**, 317-323.
51. H. G. H. van Melick, L. E. Govaert and H. E. H. Meijer, *Polymer*, 2003, **44**, 2493-2502.
52. Y. Y. Wang, S. W. Cheng and S. Q. Wang, *J. Rheology*, 2011, **55**, 1247-1270.
53. U. H. Choi and R. H. Colby, *Macromolecules*, 2017, **50**, 5582-5591.
54. U. H. Choi, A. Mittal, T. L. Price, H. W. Gibson, J. Runt and R. H. Colby, *Macromolecules*, 2013, **46**, 1175-1186.
55. J. Bartels, J. H. H. Wang, Q. Chen, J. Runt and R. H. Colby, *Macromolecules*, 2016, **49**, 1903-1910.
56. U. H. Choi, S. W. Liang, Q. Chen, J. Runt and R. H. Colby, *ACS Appl. Mater. Interfaces*, 2016, **8**, 3215-3225.
57. P. J. Yoo, K. Y. Suh, H. Kang and H. H. Lee, *Phys. Rev. Lett.*, 2004, **93**.
58. M. Watanabe, S. Nagano, K. Sanui and N. Ogata, *Solid State Ionics*, 1988, **28**, 911-917.
59. J. Evans, C. A. Vincent and P. G. Bruce, *Polymer*, 1987, **28**, 2324-2328.
60. K. E. Thomas, S. E. Sloop, J. B. Kerr and J. Newman, *J. Power Sources*, 2000, **89**, 132-138.
61. N. Boaretto, A. Bittner, C. Brinkmann, B. E. Olsowski, J. Schulz, M. Seyfried, K. Vezzu, M. Popall and V. Di Noto, *Chem. Mater.*, 2014, **26**, 6339-6350.
62. L. Porcarelli, C. Gerbaldi, F. Bella and J. R. Nair, *Sci. Rep.*, 2016, **6**.
63. C. Monroe and J. Newman, *J. Electrochem. Soc.*, 2005, **152**, A396-A404.